RSC Advances

PAPER

View Article Online
View Journal | View Issue

Cite this: *RSC Adv.*, 2022, **12**, 1005

Theoretical investigation on the effect of the ligand on bis-silylation of C(sp)–C(sp) by Ni complexes†

Li Hui, *[ab] He Yuhan[a] and Wang Jiaqi[a]

Received 7th November 2021
Accepted 21st December 2021

DOI: 10.1039/d1ra08153e

rsc.li/rsc-advances

Density functional theory is used to study the bis-silylation of alkyne catalysed by a transition metal nickel–organic complex. The active catalyst, organic ligand, reaction mechanism, and rate-determining step were discussed with regard to dynamics and thermodynamics. COD or SIPr (COD = cyclooctadiene, SIPr = 1,3-bis(2,6-diisopropyl-phenyl)-4,5-dihydroimidazol-2-ylidene) coordination with Ni will greatly reduce the energy barrier of the Si–Si insertion step, that is, $\Delta\Delta G$ reaches 15.5 kcal mol^{-1}. Furthermore, the structure of alkynes will change the energy barrier of the alkyne insertion step.

Introduction

Organosilicon compounds are widely used in organic synthetic chemistry,[1] materials science,[2] and pharmaceutical chemistry.[3] It is important to develop a rapid and efficient method for preparing silane compounds. Transition metal-catalysed bis-silylation of alkynes with disilanes, particularly chain disilanes, has received considerable interest amongst researchers.[4–6] 1, 2-Bisilicyl alkenes have wide and important application potential in the field of organic synthesis.[7–10] The two silicon pieces based on alkenes show different activities in the subsequent transformation of products, and organic molecules with various structures can be synthesised through stepwise regional and chemically selective transformation. The transition metal-catalysed bis-silylation of the alkyne is an effective method of synthesising disubstituted alkenes.[11,12] However, this method has the following limitations: the use of symmetrical ethyl silane to introduce two identical silyl groups, which can hardly distinguish the two silyl groups effectively in subsequent transformation. Transition metal complexes of platinum group metals with low valence are used as catalysts. Therefore, developing asymmetric bis-silylation catalysed by earth-abundant metal is important.

In 1994, Ozawa and co-workers[13] reported the bis-silylation of acetylene using Me_3SiSiF_2Ph as silane reagent in the presence of a palladium catalyst to construct bis-silylated olefin. In 2015, Spencer[14] reported intermolecular bis-silylation (hexamethyldisilane) catalysed by a palladium complex to construct *cis*-bis-silylation alkenes. In 2018, Song[15] used asymmetric disilane reagents for the region- and stereo-selective bis-silylation of alkynes. One Si-atom was connected to an amide group that could coordinate with transition metal Pd to achieve asymmetric di-silicification of terminal alkynes. In 2021, Zhao[16] adjusted the amide group with weak coordination ability to quinoline group 8-(2-substituted 1,1,2,2-tetramethyldisilanyl) quinoline (TMDQ). The strong coordination of TMDQ was used to form complexes with nickel to achieve Si–Si activation, and then the bis-silicification between TMDQ and various unsaturated bonds was further obtained. In addition, using quinoline as directing group, the two adjacent silicon groups in the product can be distinguished efficiently in the subsequent chemical transformation, thereby generating bis-silicon alkene products. Although many production methods can be used to construct vinylsilane, the synthesis of tetra-substituted vinylsilane remains challenging for researchers.[17–23]

Based on the above-mentioned experimental research results, the author focussed on the following contents. Introducing the directing group in silane, which can be coordinated with metal centre Ni, can improve the catalytic activity of Ni. In addition, the structure of alkynes may affect the coordination capacity and selectivity of products. The regio-selective synthesis of di-silane has always been concerned by several researchers, and many difficulties are identified during synthesis. Theoretical calculation work can provide theoretical support with guiding significance for experimental work.

Results and discussion

Ligands and coordination capacity of catalysts

As shown in Scheme 1, Zhao and co-author[16] have reported bis-silylation of internal alkynes enabled by Ni(0) catalysis. As shown in Fig. 1, **Ni1**, **Ni2** and **Ni3** are used as COD/COD, SIPr/SIPr and COD/SIPr ligands, respectively (COD = cyclooctadiene, SIPr = 1,3-bis(2,6-diisopropyl-phenyl)-4,5-dihydroimidazol-2-ylidene). In the case of **Ni1**, the multiplicity of **Ni1a** is 1, and the multiplicity of **Ni1b** is 3. In the reaction

[a]*College of Chemistry and Chemical Engineering, North Minzu University, Yinchuan, China. E-mail: lihui@nun.edu.cn*

[b]*Key Laboratory of Chemical Engineering and Technology, North Minzu University, State Ethnic Affairs Commission, Yinchuan, China*

† Electronic supplementary information (ESI) available. See DOI: 10.1039/d1ra08153e

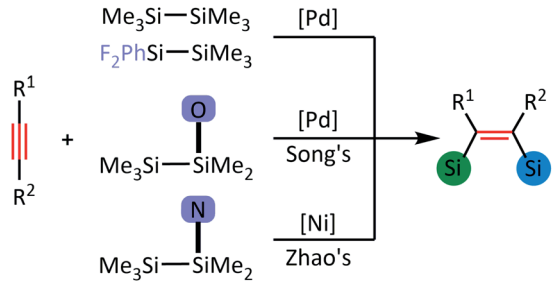

Scheme 1 Bis-silylation of alkynes with asymmetric disilanes catalysed by a transition metal.

system,[16] 10 mol% $Ni(COD)_2$ and 12 mol% SIPr were added to the reaction system, and the yield reached 98%, following the addition of SIPr compared with ICy and PPh_3.

With regards to the phenomenon, we think that the starting point of the catalytic cycle for the reaction may not be **Ni1**. Therefore, the ligands and multiplicity are discussed below. In the case of ligand exchange between the neutral ligand SIPr and COD, SIPr coordinated with Ni and generated **Ni2**, and either SIPr or COD both coordinated with Ni simultaneously and then generated **Ni3**. In addition, the electron configuration outside the nucleus of Ni is $3d^8 4s^2$, and the eight electronic configurations in the d orbital may result in the multiplicity of $Ni(COD)_2$ being 1 or 3. Meanwhile, the SIPr system shows singlet and triplet states. Furthermore, the **Ni1**, **Ni2** and **Ni3** intermediates show singlet and triplet states. Then, we label the singlet ^{1}**Ni1** state as **Ni1a**, the triplet ^{3}**Ni1** state as **Ni1b**, and the other intermediates.

$$\underset{\text{Ni1a}}{Ni(COD)_2} + 2SIPr \longrightarrow \underset{\text{Ni2a}}{Ni(SIPr)_2} + 2COD \quad (1)$$

$$\underset{\text{Ni1a}}{Ni(COD)_2} + SIPr \longrightarrow \underset{\text{Ni3a}}{Ni(COD)(SIPr)} + COD \quad (2)$$

$$\Delta G = G_{\mathbf{Ni2a}}/G_{\mathbf{Ni3a}} + nG_{\mathrm{COD}} - G_{\mathbf{Ni1a}} - nG_{\mathrm{SIPr}} \quad (3)$$

The calculated results show that the Gibbs free energy of triplet **Ni1b** is 26.9 kcal mol^{-1} higher than that of singlet **Ni1a** (**Ni1a** as the relative zero point) after correction for solvation effect. The singlet states of **Ni2a** and **Ni3a** are stable in thermodynamics (relative energy comparable to **Ni2a**/**Ni2b** and **Ni3a**/**Ni3b** in ESI†). Then, delta Gibbs free energy for reaction (1) and reaction (2) was calculated. In reaction (1), two neutral COD ligands are dissociated and coordinated with two neutral SIPr ligands. In reaction (2), one neutral molecular COD is dissociated and coordinated with one neutral molecular SIPr. The Gibbs free energy calculation formula is based on eqn (3). The delta Gibbs free energy of reaction (1) is −14.6 kcal mol^{-1}, whereas that of reaction (2) is −1.3 kcal mol^{-1}. Therefore, $Ni(SIPr)_2$ is the most stable structure. However, whether or not $Ni(SIPr)_2$ is an active catalyst remains unknown.

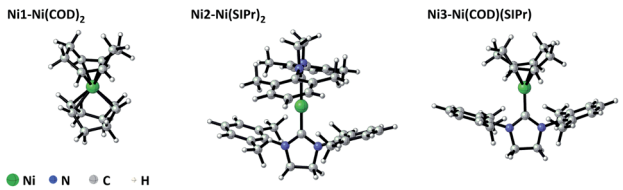

Fig. 1 Ligands and coordination complex of **Ni1**, **Ni2** and **Ni3** catalysts.

Next, the coordination capacity of Ni-atom with COD and/or SIPr in **Ni1a**, **Ni2a** and **Ni3a** catalysts was studied. The sum of natural adaptive orbital (NAdO) eigenvalues[24] of the C=C bond is 1.87382 in COD. The NAdO eigenvalue is an orbital closely related to bond order density, which can exhibit the source of delocalisation index with regards to an orbital picture. In addition, the delocalisation index is visualised and important in understanding the nature and interatomic interaction. The sum of NAdO eigenvalues of the C–N bond is 1.44774 in SIPr. By contrast, the sum of NAdO eigenvalues of the C=C bond reduces to 1.33252 after the C=C double bond as η^2 ligand coordinated with Ni-atom in the **Ni1a** complex. The sum of NAdO eigenvalues of the C–N bond decreases to 1.30377 after nitrene coordination with Ni-atom in the **Ni2a** complex. The sum of NAdO eigenvalues of the C=C double bond decreases to 1.35341, and the sum of the NAdO eigenvalues of the C–N bond decreases to 1.28442. The sum of NAdO eigenvalues of the C–Ni bond in **Ni1a** is 0.64763/0.66437/0.66454/0.64781/0.64778/0.66453/0.66472/0.64799, and the average value is 0.65617. The sum of NAdO eigenvalues of N–Ni bonds in **Ni2a** is 1.20931/1.20918, and the mean value is 1.20925. The sum of NAdO eigenvalues of N–Ni bonds in **Ni3a** is 1.22928, and that of C–Ni is 0.69151/0.68551/0.68543/0.69140. The average value is 0.68846.

Based on the NAdO value of ligands and complexes, the NAdO eigenvalues of COD and SIPr decreased because of the coordination with Ni-atoms. The C=C double bond in COD as η^2 ligands and N-atoms in SIPr were delocalised because of coordination. In addition, the coordination capacity of the C=C bond in COD is significantly stronger than that of nitrene in SIPr. Combined with the reaction mechanism and free energy surface, we hypothesise that the coordination capacity of COD is stronger than SIPr, and COD as a strong ligand 'locks up' the coordination site between Ni-atom and the substrate.

Reaction mechanism

Theoretical calculation of quinoline and dimethylacetylene was used as a model reaction to conduct a reaction mechanism study under optimal reaction conditions. **R1** generation Pro catalysed by $Ni(COD)_2$ and SIPr is shown in Fig. 2. The reaction consists of three steps, oxidation addition/Si–Si bond broken, alkyne insertion/C≡C activation, and reductive elimination. The metal centre Ni of the catalyst underwent Ni^0–Ni^{II}–Ni^0 during the catalytic cycle. The N-atom coordination with Ni in TMDQ effectively controlled the catalytic activity of catalyst centre Ni-atom.

As shown in Fig. 2, intermediate **INT1a** was formed by coordination of Ni-atom in catalyst and N-atom in reagent **R1**.

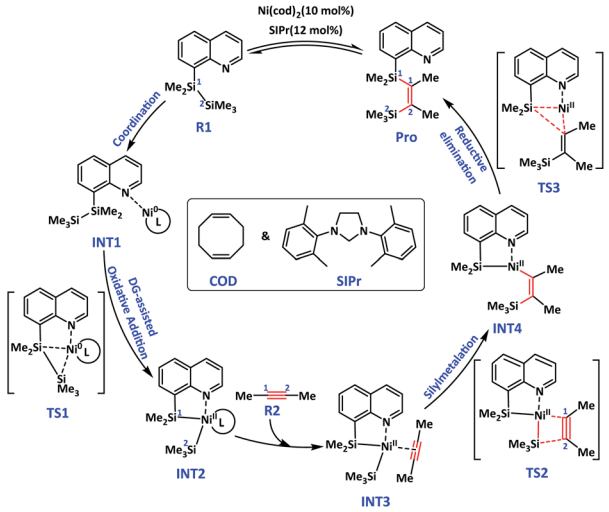

Fig. 2 Bis-silylation reaction mechanism of quinoline and dibenzenyl catalysed by Ni-complexes.

Then, the Si–Si bond oxidative addition was catalysed by the Ni-complex, which underwent ternary ring transition state **TS1** by breaking the Si1–Si2 bond and generating the Si1–Ni–Si2 bond. In the Si–Si oxidative step, the Si1 atom attacked the Ni atom, and then a three-membered ring was formed. The distance of Si1–Ni from 4.54 Å in **INT1a** decreased to 2.65 Å in **TS1a** and then further decreased to 2.23 Å in **INT2a**. Meanwhile, the distance of Si2–Ni from 6.77 Å in **INT1a** decreased to 2.62 Å in **TS1a** and then further decreased to 2.28 Å in **INT2a**. We hypothesise that the N-atom coordination with Ni in **TMDQ** controlled the catalytic activity of catalyst centre Ni-atom. The bond length of Ni–N is 1.94, 1.97 and 2.05 Å in **INT1a**, **TS1a** and **INT2a**, respectively. Evidently, the generation of the Si1–Ni–Si2 bond weakens the chemical bond strength of the Ni–N bond. The bond length of Si1–Si2 is 2.38, 2.43 and 2.80 Å in **INT1a**, **TS1a** and **INT2a**, respectively.

The transition metal centre Ni^0 is oxidised to Ni^{II} form the cyclometallation intermediate **INT2**. The intermediate **INT3** is formed after alkyne(**R2**) coordination with Ni in **INT2**, which occurs during the alkyne insertion reaction. The C≡C in **R2** as η^3 ligand coordinated with Ni-atom in **INT2a**, followed by dissociation of COD, and then generation **INT3a**. In **INT3a**, the bond length of Ni–C1, Ni–C2 and C1–C2 is 1.92, 1.89 and 1.28 Å, respectively. Compared with the coordination of C=C in COD with Ni in **INT2a**, C≡C coordination with Ni in **INT3a** is markedly enhanced. After C≡C in **R2** coordinated with Ni, the bond length increased from 1.21 Å to 1.28 Å. The intermolecular silylmetalation reaction *via* Ni–C1–C2–Si2 quaternary ring transition state **TS2** forms the intermediate **INT4**. The bond length of C1–C2 is 1.28, 1.32 and 1.41 Å in **INT3a**, **TS2a** and **INT4a**, respectively. In addition, the bond length of Ni–N is 2.03, 1.97, 2.05 and 2.09 Å in **INT3a**, **TS2a**, **INT4a** and **INT4c**, respectively. Therefore, the N-atom modulated the coordination activity of Ni-atom, and SIPr had a stronger coordination capacity than COD, thereby leading to a longer bond length in Ni–N(8-Qu). Then, Then, COD or coordination with Ni-atom could ensure coordinative saturation in **INT4a**/**INT4c**. Reductive elimination of **INT4a** is accompanied by Si1–Ni–C1 three-membered ring transition state of **TS3**, generating the bis-silylation product **Pro**. Meanwhile, the Ni^0 catalyst is regenerated.

The free energy surface (Fig. 3) serves (**Ni1a** + **R1**) as the relative zero point. All the energies were corrected by using

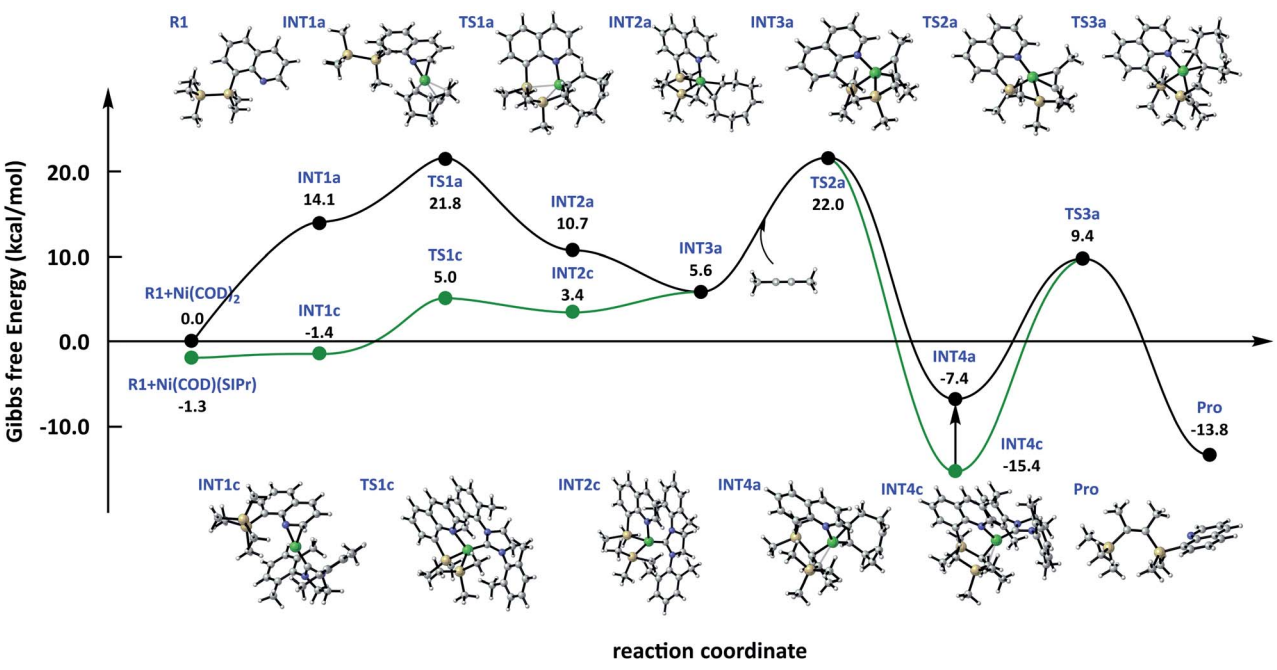

Fig. 3 Free energy surface of bis-silylation of the C(sp)–C(sp) bond catalysed by the Ni complex was corrected by SMD solvation model in toluene.

a continuum solvation model based on density (SMD)[25] in toluene (the free energy surface in a vacuum is shown in Fig.-SI†). As shown in Fig. 3, the energy span of the oxidation addition step is 6.3 kcal mol^{-1} using **Ni3a** as catalyst, whereas the energy barrier is 21.8 kcal mol^{-1} using **Ni1a** as the catalyst. The calculation results are in consistent with our prediction about active catalysts either from thermodynamics or kinetics. Next, the same mechanism in alkyne insertion steps is observed, and the energy barrier is 16.4 kcal mol^{-1}. Considering that SIPr has a stronger coordination capacity than COD, **INT4c** is 8.0 kcal mol^{-1} lower than **INT4a**. Therefore, COD coordination with Ni is the suitable path, whose energy barrier is 16.8 and 24.8 kcal mol^{-1} from **INT4a** and **INT4c** to **Pro** in the reductive elimination step, respectively. Therefore, using **Ni3a** as the catalyst is more advantageous than **Ni1a**, and the rate-determining step is a reductive elimination step.

Disparity of alkyne structure during alkyne insertion

Theoretical calculations were performed for the three representative alkynes, namely, **R2a**, **R2b** and **R2c**, to investigate the influence of the alkyne structure on alkyne silylmetalation during alkyne insertion. As shown in Fig. 4, the alkynes **R2a** and **R2b** have a symmetric structure, and **R2c** has asymmetric substitution. These three alkyne structures are selected to explore the influence of aliphatic substituent methyl and aromatic substituent phenyl connected to the C≡C triple bond and to study the interaction between Me/Ph and the C≡C triple bond. We hypothesise that the reaction energy barrier and selectivity might affect the alkyne insertion reaction.

Firstly, the Mulliken charge was calculated for sp-C in **R2a**, **R2b** and **R2c**, and the values are 0.032, 0.163 and 0.136/0.197, respectively. In addition, the nucleophilicity of phenyl is stronger than that of methyl. The π electron conjugation between phenyl and C≡C has evident delocalisation characteristics. Meanwhile, the Mulliken charge of C1-atom connected to –Me in **R2c** is 0.136, and that of C2-atom connected to –Ph is 0.197. The charge is redistributed because of the substitution of Me and Ph in C1≡C2. The locally delocalised frontier molecular orbital indicating π–π conjugation of C≡C and phenyl and the electron cloud are biased towards phenyl in **R2c**. Based on the characteristics of electron-delocalised conjugation, the conjugation of C1≡C2 and –Ph might affect the selectivity of alkyne insertion.

The coordination of Ni-atom with N-atom in the N heterocyclic segment in **R1** will directly affect the catalytic activity and will determine whether the sites for the C≡C triple bond coordination with Ni-atom are adequate. Then, hole–electron analysis was used to investigate electron excitation characteristics in substrates. The contribution of the substituent group for HOMO in **R2a**, **R2b** and **R2c** is shown in Fig. 5. The exciton binding energy (coulomb attraction energy) is 8.98 eV in **R2a**; the orbital delocalisation index (ODI) of methyl is 29.72% for HOMO, and the fragment contribution and ODI of the fragment are 12.131% and 35.31%, respectively. Therefore, the C≡C triple bond forms a distinct π bond in HOMO, and the methyl group is in a relatively independent state. The exciton binding energy is 6.35 eV in **R2b**; the ODI of phenyl is 24.83% for HOMO, and the fragment contribution and ODI of the fragment are 92.96% and 28.34%, respectively. Therefore, a delocalised π–π bond formatted between C≡C and phenyl contributed greatly to HOMO. The exciton binding energy is 6.60 eV in **R2c**; the ODI of methyl/phenyl is 24.88%/24.88% for HOMO; the fragment contribution is 0.17%/93.12%, and the ODI of the fragment is 51.20%/28.28%.

The restrained electrostatic potential (RESP)[26] charge was used to study **R2a**, **R2b** and **R2c** reactants. Fitting the electrostatic potential charge near and outside the van der Waals surface of the molecule calculated on the basis of the wave function reproduces an atomic charge, which is graphically displayed as RESP. In **R2a**, the minimum electrostatic potential point (blue area) is concentrated nearby the C≡C triple bond, and the minimum value is −19.47 kcal mol^{-1}. In the **R2b** reactant, the minimum value of the C≡C fragment is −15.81 kcal mol^{-1}. In the **R2c** reactant, the minimum value of C≡C is −19.32 kcal mol^{-1}. The C≡C triple bond must coordinate with metal Ni in the following step. The calculation results indicated that **R2b** had the lowest RESP charge compared with the other two substrates, in which the conjugation of phenyl led to weakness coordination, making it conducive to subsequent alkyne insertion.

We conducted transition state search and activation energy calculation for alkyne insertion to elucidate the effect of the alkyne structure on the reaction energy barrier and the influence of asymmetric alkyne on selectivity. As shown in Fig. 6, **INT3c** and **INT3d** are intermediates coordinated by methyl-phenyl-acetylene (**R2c**) and Ni-atom, and **INT3e** is an intermediate coordinated by dibenzenyl (**R2b**) and Ni-atom. The free energy surface of **INT3** to **TS2** serves (**Ni1a** + **R1**) as the relative zero point. The binding energy of complexes increases significantly (Δ*G* increases) after phenyl appears in alkynes, indicating that the stagnation point of **INT3c**, **INT3d** and **INT3e** has a lower

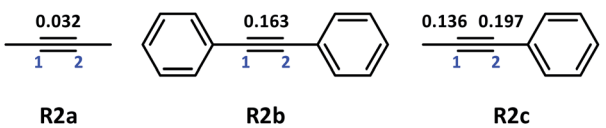

Fig. 4 Structure and Mulliken charges of C1≡C2 in **R2a**, **R2b** and **R2c**.

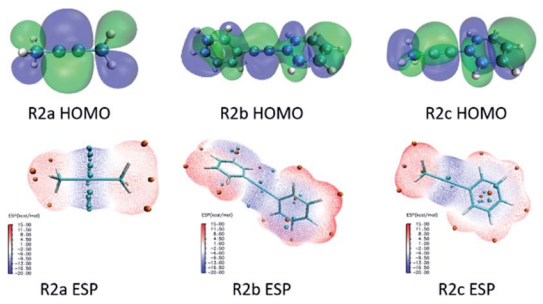

Fig. 5 Contribution of the substituent group for HOMO in **R2a**, **R2b** and **R2c**, and restrained electrostatic potential (RESP) surface in **R2a**, **R2b** and **R2c**.

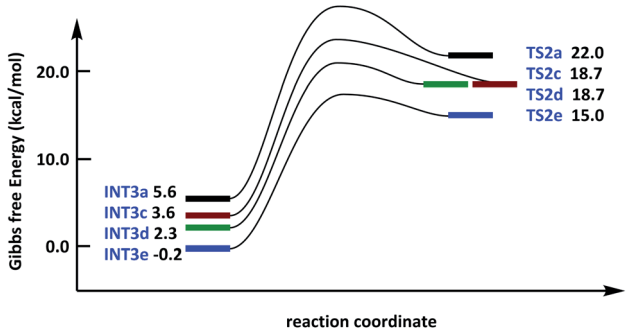

Fig. 6 Free energy surface of bis-silylation of the C(sp)–C(sp) bond catalysed by the Ni complex was corrected by SMD solvation model in toluene.

Gibbs free energy than **INT3a**. In addition, the coordination direction of C1–C2 is flipped in **R2c**, and the delta relative energy of **INT3c** and **INT3d** is 1.3 kcal mol^{-1}. Moreover, **INT3d** has lower relative energy because of the presence of π–π conjugation between 8-Qu in **R1** and phenyl in **R2c** (Fig. 6). The energy barrier of intermediates **INT3c**/**INT3d** to **TS2c**/**TS2d** is 15.1 and 16.4 kcal mol^{-1}, respectively. Furthermore, the bond length of Ni–Si from 2.29/2.28 Å increased to 2.41/2.38 Å compared with **INT3a** → **TS2a** (2.28 Å to 2.38 Å) and **INT3e** → **TS2e** (2.29 Å to 2.42 Å). Therefore, the bond length in the substrate and the structure in the transition state are due to the coordination capacity, which leads to the difference in energy barrier. In addition, phenyl-substituted alkynes have the lowest reaction energy barrier during alkyne insertion.

Conclusions

Density functional theory calculation results of TMDQ and alkyne show that the reaction consists of three steps, oxidation addition, alkyne insertion and reductive elimination. The metal centre Ni of the catalyst underwent Ni^0–Ni^{II}–Ni^0 during the catalytic cycle. In addition, the N-atom coordination with Ni in TMDQ effectively controlled the catalytic activity of the catalyst centre Ni-atom. The alkyne insertion step is closely related to the coordination intensity between the catalyst Ni and C≡C triple bond. Phenyl-substituted alkynes have the lowest reaction energy barrier during alkyne insertion. Moreover, the coordination capacity of the C=C bond in COD is significantly stronger than that of nitrene in SIPr, and COD as a strong ligand 'locks up' the coordination site between Ni-atom and the substrate.

Computational details

All the optimised structures and frequency analysis were calculated at the B3LYP/BSI level using hybrid DFT[27] implemented in Gaussian 09.[28] BSI denotes the SDD[29] basis set for Ni and the 6-31G(d)[30] basis set for the other atoms (H, C, N and Si). The transition states were further confirmed by vibrational analysis and characterised by using only imaginary frequencies. Intrinsic reaction coordinate calculations were performed to confirm the INTs along the reaction pathway. Optimised structures and frequency analysis calculations were conducted using the SMD to evaluate the effects of the solvent on the potential energy surface. The ωB97X-D/BSII level[31,32] was used to calculate solvation single-point energies and provide accurate energy information, in which BSII denotes the SDD basis set for Ni and the 6-311 + G(d, p)[33] basis set for the other atoms (H, C, N and Si). The hybrid density functional B3LYP and ωB97X-D method is reliable, which has been used in previous studies.[34–36] Moreover, SDD is suitable for the Ni-atom. The energies discussed in this paper are Gibbs free energies (kcal mol^{-1}) in the solution. The importance of orbital wavefunction in the plane was drawn by Multiwfn.[37]

Author contributions

The manuscript was written through contributions of all authors. All authors have given approval to the final version of the manuscript.

Conflicts of interest

The authors declare no competing financial interest.

Acknowledgements

This work was supported by Science and Technology Research Project of Ningxia Institution Foundation (No. NGY2018-145), Natural Science Foundation of Ningxia Province (2019AAC03140, 2018AAC03251), the National Natural Science Foundation of China (21963001), and Ningxia low-grade resource high value utilization and environmental chemical integration technology innovation team project, China.

Notes and references

1 K. Matsuoka, N. Komami, M. Kojima, T. Mita, K. Suzuki, S. Maeda, T. Yoshino and S. Matsunaga, *J. Am. Chem. Soc.*, 2021, **143**, 103.
2 A. P. Amrute, B. Zibrowius and F. Schüth, *Chem. Mater.*, 2020, **32**, 4699.
3 S. Guariento, M. Biagetti and P. Ronchi, *Future Med. Chem.*, 2021, **13**, 595.
4 W. Gao and S. Ding, *Synthesis*, 2020, **52**, 3549.
5 T. Fuchigami and S. Inagi, *Curr. Opin. Electrochem.*, 2020, **24**, 24.
6 F. Ye, Z. Xu and L. W. Xu, *Acc. Chem. Res.*, 2020, **54**, 452.
7 R. Waterman, P. G. Hayes and T. D. Tilley, *Acc. Chem. Res.*, 2007, **40**, 712.
8 F. M. Mück, J. A. Baus, R. Bertermann, C. Burschka and R. Tacke, *Organometallics*, 2016, **35**, 2583.
9 Y. Wang, H. P. Hickox, Y. Xie, P. Wei, H. F. Schaefer III and G. H. Robinson, *J. Am. Chem. Soc.*, 2017, **139**, 16109.
10 C. Xu, Z. Ye, L. Xiang, S. Yang, Q. Peng, X. Leng and Y. Chen, *Angew. Chem., Int. Ed.*, 2021, **60**, 3189.

11 N. Lassauque, P. Gualco, S. Mallet-Ladeira, K. Miqueu, A. Amgoune and D. Bourissou, *J. Am. Chem. Soc.*, 2013, **135**, 13827.
12 J. Li, Y. Li, I. Purushothaman, S. De, B. Li, H. P. Zhu, P. Parameswaran, Q. S. Ye and W. P. Liu, *Organometallics*, 2015, **34**, 4209.
13 F. Ozawa, M. Sugawara and T. Hayashi, *Organometallics*, 1994, **13**, 3237.
14 M. B. Ansell, D. E. Roberts, F. G. N. Cloke, O. Navarro and J. Spencer, *Angew. Chem., Int. Ed.*, 2015, **54**, 5578.
15 P. Xiao, Y. Cao, Y. Gui, L. Gao and Z. Song, *Angew. Chem., Int. Ed.*, 2018, **130**, 4859.
16 Y. Zhang, X. C. Wang, C. W. Ju and D. Zhao, *Nat. Commun.*, 2021, **12**, 1.
17 T. A. Blumenkopf and L. E. Overman, *Chem. Rev.*, 1986, **86**, 857.
18 D. S. W. Lim and E. A. Anderson, *Synthesis*, 2012, **44**, 983.
19 M. Zhang, Y. Zhang, X. Jie, H. Zhao, G. Li and W. Su, *Org. Chem. Front.*, 2014, **1**, 843.
20 R. Shintani, H. Kurata and K. Nozaki, *J. Org. Chem.*, 2016, **81**, 3065.
21 T. Iwamoto, T. Nishikori, N. Nakagawa, H. Takaya and M. Nakamura, *Angew. Chem., Int. Ed.*, 2017, **129**, 13483.
22 T. He, L. C. Liu, L. Guo, T. He, L. C. Liu and L. Guo, *Angew. Chem., Int. Ed.*, 2018, **130**, 11034.
23 M. F. Wisthoff, S. B. Pawley, A. P. Cinderella and D. A. Watson, *J. Am. Chem. Soc.*, 2020, **142**, 12051.
24 J. L. Casals-Sainz, A. Fernández-Alarcón, E. Francisco, A. Costales and A. M. Pendás, *J. Phys. Chem. A*, 2019, **124**, 339.
25 A. V. Marenich, C. J. Cramer and D. G. Truhlar, *J. Phys. Chem. B*, 2009, **113**, 6378.
26 C. I. Bayly, P. Cieplak, W. Cornell and P. A. Kollman, *J. Phys. Chem.*, 1993, **97**, 10269.
27 J. A. Pople, P. M. W. Gill and B. G. Johnson, *Chem. Phys. Lett.*, 1992, **199**, 557.
28 J. E. Peralta Jr, F. Ogliaro, M. Bearpark, J. J. Heyd, E. Brothers, K. N. Kudin, V. N. Staroverov, T. Keith, R. Kobayashi, J. Normand, K. Raghavachari, A. Rendell, J. C. Burant, S. S. Iyengar, J. Tomasi, M. Cossi, N. Rega, J. M. Millam, M. Klene, J. E. Knox, J. B. Cross, V. Bakken, C. Adamo, J. Jaramillo, R. Gomperts, R. E. Stratmann, O. Yazyev, A. J. Austin, R. Cammi, C. Pomelli, J. W. Ochterski, R. L. Martin, K. Morokuma, V. G. Zakrzewski, G. A. Voth, P. Salvador, J. J. Dannenberg, S. Dapprich, A. D. Daniels, O. Farkas, J. B. Foresman, J. V. Ortiz, J. Cioslowski and D. J. Fox, *Gaussian 09*, Revision D.01, Wallingford CT, 2013.
29 T. H. Dunning Jr and P. J. Hay, *Modern Theoretical Chemistry*, ed. H. F. Schaefer III, vol. 3, Plenum, New York, 1976, pp. 1–28.
30 G. A. Petersson and M. A. Al-Laham, *J. Chem. Phys.*, 1991, **94**, 6081.
31 R. G. Parr and W. Yang *Density Functional Theory of Atoms and Molecules*, Oxford University Press, Oxford, U.K. 1989.
32 T. Ziegler, *Chem. Rev.*, 1991, **91**, 651.
33 L. A. Curtiss, M. P. McGrath, J. P. Blaudeau, N. E. Davis, R. C. Binning Jr and L. Radom, *J. Chem. Phys.*, 1995, **103**, 6104.
34 H. Li, X. Ma, B. Zhang and M. Lei, *Organometallics*, 2016, **35**, 3301.
35 H. Li, X. Ma and M. Lei, *Dalton Trans.*, 2016, **45**, 8506.
36 H. Li, W. Tang and Z. Ma, *Dalton Trans.*, 2021, **50**, 10291.
37 T. Lu and F. Chen, *J. Comput. Chem.*, 2012, **33**, 580.